Journal of Statistical Physics, Vol. 121, Nos. 1/2, October 2005 (© 2005)
DOI: 10.1007/s10955-005-5963-z

Lattice Boltzmann Simulation of Shear-Thinning Fluids*

Dirk Kehrwald[1]

Received October 12, 2004; accepted May 5, 2005

It is shown how shear-thinning flow can be simulated without the need for numerical differentiation by following a lattice Boltzmann approach. The basic idea of is to combine the Cross model of viscosity with a 3D multiple relaxation time lattice Boltzmann method and to extract the required velocity derivatives from intrinsic quantities of the lattice Boltzmann scheme. Computational results are presented for a simple benchmark and for the simulation of liquid composite moulding.

KEY WORDS: Lattice Boltzmann methods; shear-thinning fluids; liquid composite moulding.

1. INTRODUCTION

The aim of the present paper is to assess the capability of the relatively new and increasingly popular lattice Boltzmann methods to solve practically relevant problems in a very convincing way. In particular, it will be demonstrated how to avoid the troublesome procedure of numerical differentiation during the simulation of shear-thinning fluids by following a lattice Boltzmann approach.

Fluids such as water and glycerin, whose shear stress is at constant temperature proportional to the rate-of-strain, are referred to as Newtonian fluids and their flow is governed by the classical Navier–Stokes equations. Any fluid that is not governed by the Newtonian relation of shear stress and rate-of-strain, e.g. blood plasma, tooth-paste, egg-white,

*Extended version of a talk presented at ICMMES 2004, Braunschweig, Germany, July 2004.
[1]Fraunhofer-Institut für Techno- und Wirtschaftsmathematik, Gottlieb-Daimler-Straße, Geb. 49, D-67663 Kaiserslautern, Germany; e-mail: kehrwald@itwm.fraunhofer.de

corn starch suspensions, and ketchup, is called non-Newtonian. The science studying the behaviour of such fluids is called rheology. According to their behaviour, non-Newtonian fluids are subdivided into several groups, among them visco-plastic (e.g. tooth-paste), visco-elastic (e.g. egg-white), shear-thickening (e.g. corn starch suspensions), and shear-thinning (e.g. ketchup) fluids.

One class of shear-thinning fluids are the *in situ* polymerising polyamides used in liquid composite moulding.[19,20] However, software tools for simulating liquid composite moulding are typically based on Darcy's law,[4] which relates the flow rate of a Newtonian fluid in a porous medium to the pressure drop across the medium. As a first step towards establishing a Darcy-like law for shear-thinning fluids, the present paper describes a stable and robust numerical method for simulating shear-thinning flow in complex geometries, such as the fibre beds used in liquid composite moulding. However, the mathematical model considered in the following neglects the eventual solidification of *in situ* polymerising polyamides during the moulding process, so comparisons to laboratory measurements do not make sense at the current stage of this research.

For a shear-thinning fluid, viscosity depends on certain derivatives of the velocity field. A straightforward idea for computing those derivatives would be to numerically differentiate the velocity field obtained by the flow solver. The main difficulty of this approach is that, due to the nature of differentiation itself, it is instable in the sense that small perturbations in the initial data lead to large deviations in the solution. However, Ginzburg and Steiner[7] demonstrated how those derivatives can be obtained in lattice Boltzmann methods by straight calculation without numerical differentiation. Because of this feature, lattice Boltzmann schemes are particularly suitable for the simulation of shear-thinning flow. Note that by choosing an appropriate viscosity function, the method presented below can be adopted straightforwardly to shear-thickening flow.

In general, lattice Boltzmann methods are widely believed to offer excellent possibilities for simulating non-Newtonian flow. In 1993, Aharonov and Rothman,[1] who also considered shear-thinning flow, as well as d'Humières and Lallemand[13] published the first papers on the subject, Giraud, d'Humières, and Lallemand[9,10] developed a 2D lattice Boltzmann model of visco-elastic flow, and Lallemand *et al.*[17] provided a 3D one. Ginzburg and Steiner[7] considered lattice Boltzmann schemes for visco-plastic flow. In contrast to the approach by Aharonov and Rothman, the work presented below is based on the more realistic Cross model instead of a simple power law, uses a more elaborate lattice Boltzmann scheme, and pays due attention to stable and efficient computation of velocity derivatives.

A relatively detailed overview of the voluminous work done in numerical simulation of non-Newtonian fluids is given by Owens and Phillips.[18]

The article is structured as follows. Section 2 gives an overview of mathematical modelling of shear-thinning fluids, while Section 3 contains a general introduction to lattice Boltzmann methods. In Section 4, it is shown how lattice Boltzmann methods can be applied to the simulation of shear-thinning flow without making use of numerical differentiation, and Section 5 presents computational results for a simple benchmark problem (Section 5.1) and the simulation of liquid composite moulding (Section 5.2). Conclusions are then drawn in Section 6.

In the following, summation is implicitly assumed over repeated Greek but not Latin indices. The present paper concentrates on Stokes flow but all the models and methods can be applied to the Navier–Stokes regime as well.

2. MATHEMATICAL MODEL

Slowly moving incompressible fluids in a domain $[0, T] \times \Omega$ with $T \in \mathbb{R}_+$ and $\Omega \subset \mathbb{R}^d$, $d = 2, 3$, are typically modelled by the time-dependent Stokes equations

$$\partial_\alpha u_\alpha = 0 \qquad \text{and} \qquad \partial_t(\varrho u_\alpha) + \varrho F_\alpha = \partial_\beta \sigma_{\alpha\beta}, \tag{1}$$

where $\alpha, \beta = 1, \ldots, d$ denote the Cartesian coordinate directions in $\mathbb{R}^d$, ∂_α, ∂_β, etc., respectively, stand for the space derivative in direction α, β, etc., ∂_t represents the time derivative, ϱ is the constant density of the fluid, u_α represents the αth component of the velocity vector $\boldsymbol{u}$, and F_α stands for the αth component of the constant external acceleration vector $\boldsymbol{F}$. Fluids for which the stress tensor $\sigma_{\alpha\beta}$ takes the form

$$\sigma_{\alpha\beta} = -p\delta_{\alpha\beta} + \mu(\partial_\alpha u_\beta + \partial_\beta u_\alpha)$$

with pressure p and constant viscosity $\mu > 0$ are referred to as *Newtonian* and all others are called *non-Newtonian*.

It has been found by experiments that there are many fluids, especially liquid polymers, for which the viscosity μ is a linearly decreasing function of the shear rate

$$\dot{\gamma}(\boldsymbol{u}) = \sqrt{\frac{1}{2}(\partial_\beta u_\alpha + \partial_\alpha u_\beta)(\partial_\alpha u_\beta + \partial_\beta u_\alpha)}$$

tending to some limit μ_∞ for $\dot{\gamma} \to \infty$,[18] as exemplified in Fig. 1. Such fluids are called *shear-thinning* or *pseudo-plastic*. There are several approaches to modelling shear-thinning behaviour, e.g. the simple power law model[1]

$$\mu(\dot{\gamma}) = C_{pl}\dot{\gamma}^{m_{pl}-1},$$

where C_{pl} and m_{pl} are constants, the Carreau–Yasuda model[24]

$$\mu(\dot{\gamma}) = \mu_\infty + (\mu_0 - \mu_\infty)\Big(1 + (C_{CY}\dot{\gamma})\Big)^{m_{CY}/a},$$

with constants $\mu_0 = \mu(0)$, $\mu_\infty = \lim_{\dot{\gamma}\to\infty}\mu(\dot{\gamma})$, C_{CY}, m_{CY}, and a, as well as the Cross model[3]

$$\mu(\dot{\gamma}) = \mu_\infty + \frac{\mu_0 - \mu_\infty}{1 + (C\dot{\gamma})^m}, \tag{2}$$

where again $\mu_0 = \mu(0)$ and $\mu_\infty = \lim_{\dot{\gamma}\to\infty}\mu(\dot{\gamma})$, while C and m are further constants. Note that Cross model and Carreau–Yasuda approach are able to predict the Newtonian plateaus at very high and very low shear-rates (cf. Fig. 1), while the power law model is suitable only for the shear-thinning region in between. In the following, the Cross model is used exclusively. However, exchanging the viscosity model is straightforward in lattice Boltzmann simulations.

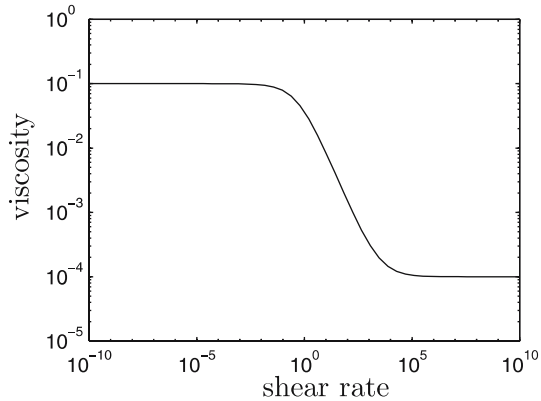

Fig. 1. The viscosity function of a typical shear-thinning fluid. Note the Newtonian behaviour for very small and very large shear rates, and the logarithmic scale on both axes.

3. LATTICE BOLTZMANN APPROACH

The lattice Boltzmann method[21--23] is a relatively new and innovative numerical approach for solving the time-dependent Stokes equations (1). The main idea of this approach is not to solve equations (1) directly but to simulate particle dynamics on a mesoscopic scale. The solution of the macroscopic Stokes equations is then obtained from discrete moments of the mesoscopic quantities (see below). Note that after a simple modification, this method solves the Navier–Stokes equations instead of the much simpler Stokes equations (1).

In lattice Boltzmann schemes, it is typically assumed that the spatial domain $\Omega \subset \mathbb{R}^d$ is covered by a lattice with equidistant nodes.[2] The set of these nodes is referred to as $\mathcal{X}$. At a given time t, the particle densities $f_j(t, \boldsymbol{x}) = f(t, \boldsymbol{x}; \boldsymbol{c}_j)$ of fluid particles located at position $\boldsymbol{x} \in \mathcal{X}$ and moving with velocity $\boldsymbol{c}_j \in \mathcal{V}_q$ are examined, where $\mathcal{V}_q = \{\boldsymbol{c}_j : j = 0, \ldots, q-1\}$ with some $q \in \mathbb{N}$ contains only a finite number of velocity vectors.

The evolution of particle density $f_j(t, \boldsymbol{x})$ is described by the lattice Boltzmann equation[12]

$$\begin{aligned} f_j(t+\delta t, \boldsymbol{x}+\delta t \boldsymbol{c}_j) = {} & f_j(t, \boldsymbol{x}) \\ & + \delta t \sum_{k,l} \lambda_k \Big(f_l(t, \boldsymbol{x}) - f_l^{\mathrm{eq}}(\rho(t, \boldsymbol{x}), \boldsymbol{m}(t, \boldsymbol{x})) \Big) e_{k;l} e_{k;j} \\ & + 3\delta t f_j^* c_{j;\alpha} F_\alpha, \end{aligned}$$

where λ_k are the eigenvalues of the so-called collision matrix A and $\boldsymbol{e}_k$ are the corresponding eigenvectors. Notations like $e_{k;l}$, $c_{j;\alpha}$, etc. stand for the lth component of the vector $\boldsymbol{e}_k$, the αth component of the vector $\boldsymbol{c}_j$, etc., and

$$m_\alpha(t, \boldsymbol{x}) = \sum_j c_{j;\alpha} f_j(t, \boldsymbol{x}).$$

Furthermore, f_j^* are model dependent weights, F_α stands for the constant external acceleration vector that already appeared in the Stokes equations (1), and

$$f_j^{\mathrm{eq}}(\rho, \boldsymbol{m}) = f_j^* \left(\rho + 3 m_\alpha c_{j;\alpha} \right).$$

[2] In fact, there are lattice Boltzmann schemes where this assumption is no longer maintained, see e.g. Succi[22] for an overview. However, this paper is restricted to the classical approach, where equidistant lattice nodes are assumed.

The macroscopic variables ρ and u_α are obtained via[2,6]

$$\rho(t,\boldsymbol{x}) = \sum_j f_j(t,\boldsymbol{x}) \qquad \text{and} \qquad u_\alpha(t,\boldsymbol{x}) = \frac{m_\alpha(t,\boldsymbol{x})}{\rho(t,\boldsymbol{x})} - \frac{F_\alpha}{2}, \tag{3}$$

while pressure p can be computed by

$$p(t,\boldsymbol{x}) = \frac{1}{3}\left(\rho(t,\boldsymbol{x}) - \varrho\right),$$

where ϱ represents the constant density of the incompressible fluid.

In the following, exclusively a regular cubic lattice in three space dimensions will be used, with $q = 15$ and

$$\begin{aligned}
&\boldsymbol{c}_0 = (0,0,0)^T, \quad \boldsymbol{c}_{1,3} = \pm(1,0,0)^T, \quad \boldsymbol{c}_{2,4} = \pm(0,1,0)^T,\\
&\boldsymbol{c}_{5,6} = \pm(0,0,1)^T, \quad \boldsymbol{c}_{7,13} = \pm(1,1,1)^T, \quad \boldsymbol{c}_{8,14} = \pm(-1,1,1)^T,\\
&\boldsymbol{c}_{9,11} = \pm(-1,-1,1)^T, \quad \boldsymbol{c}_{10,12} = \pm(1,-1,1)^T.
\end{aligned}$$

Following Ginzburg and Steiner,[8] the eigenvalues λ_k are chosen such that

$$\lambda_{0,1,2,3} = 0, \quad \lambda_{4,5,6,7,8} = \lambda^\mu, \quad \lambda_9 = \lambda^a, \quad \lambda_{10,11,12} = \lambda^b, \quad \lambda_{13} = \lambda^c, \quad \lambda_{14} = \lambda^d$$

with corresponding eigenvectors

$$e_{0;j} = \frac{1}{\sqrt{15}}, \quad e_{1;j} = \frac{1}{\sqrt{10}} c_{j;1}, \quad e_{2;j} = \frac{1}{\sqrt{10}} c_{j;2}, \quad e_{3;j} = \frac{1}{\sqrt{10}} c_{j;3},$$

$$e_{4;j} = 18\sqrt{2} f^*(\boldsymbol{c}_j) c_{j;1} c_{j;2}, \quad e_{5;j} = 18\sqrt{2} f^*(\boldsymbol{c}_j) c_{j;2} c_{j;3}, \tag{4a}$$

$$e_{6;j} = 18\sqrt{2} f^*(\boldsymbol{c}_j) c_{j;1} c_{j;3}, \quad e_{7;j} = \frac{27}{2\sqrt{3}} f^*(\boldsymbol{c}_j) \left(c_{j;1}^2 - \frac{\|\boldsymbol{c}_j\|_2^2}{3} \right), \tag{4b}$$

$$e_{8;j} = \frac{9}{2} f^*(\boldsymbol{c}_j) \left(c_{j;2}^2 - c_{j;3}^2 \right), \quad e_{9;j} = \frac{3}{\sqrt{8}} f^*(\boldsymbol{c}_j) c_{j;1} c_{j;2} c_{j;3}, \tag{4c}$$

$$e_{10;j} = \frac{9}{\sqrt{10}} f^*(\boldsymbol{c}_j) \left(2c_{j;1}^3 - 3c_{j;1} \left(c_{j;2}^2 + c_{j;3}^2 \right) \right),$$

$$e_{11;j} = \frac{9}{\sqrt{10}} f^*(\boldsymbol{c}_j) \left(2c_{j;2}^3 - 3c_{j;2} \left(c_{j;1}^2 + c_{j;3}^2 \right) \right),$$

$$e_{12;j} = \frac{9}{\sqrt{10}} f^*(\boldsymbol{c}_j) \left(2c_{j;3}^3 - 3c_{j;3} \left(c_{j;1}^2 + c_{j;2}^2 \right) \right),$$

$$e_{13;j} = \frac{1}{\sqrt{18}} f^*(\boldsymbol{c}_j) \left(\|\boldsymbol{c}_j\|_2^2 - 1 \right), \quad e_{14;j} = \begin{cases} 1/\sqrt{10} & \text{for } j = 1, \ldots, 6 \\ -2/\sqrt{90} & \text{otherwise.} \end{cases}$$

Note that

$$\lambda^{\mu} = -2/(6\mu + 1) \tag{5}$$

and $\lambda^{a,b,c,d}$ are very often set to -1.

4. LATTICE BOLTZMANN MODEL OF SHEAR-THINNING FLUIDS

Consistency of the lattice Boltzmann equation can be analysed either by direct asymptotic analysis,[15] by a moments approach,[14] or by Chapman–Enskog analysis.[5] Chapman–Enskog analysis is based on an asymptotic expansion of f_j around f_j^{eq},

$$f_j(t, \boldsymbol{x}) = f_j^{\mathrm{eq}}(\rho(t, \boldsymbol{x}), \boldsymbol{m}(t, \boldsymbol{x})) + \varepsilon f_j^{(1)}(t, \boldsymbol{x}) + \varepsilon^2 f_j^{(2)}(t, \boldsymbol{x}) + \mathcal{O}\left(\varepsilon^3\right), \tag{6}$$

with a small parameter ε. In this context, it can be shown that[8]

$$\varepsilon f_j^{(1)} = \frac{3}{\lambda^{\mu}} \left(c_{j;\alpha} c_{j;\beta} - \frac{\|\boldsymbol{c}_j\|_2^2}{3} \delta_{\alpha\beta} \right) f_j^* \partial_\alpha m_\beta + \frac{1}{\lambda^c} \left(\|\boldsymbol{c}_j\|_2^2 - 1 \right) f^*(\boldsymbol{c}_j) \partial_\alpha m_\alpha,$$

and using Eqs. (4) it turns out that

$$\begin{aligned}
\lambda^{\mu} \sum_j \varepsilon f_j^{(1)} e_{4,j} / \|\boldsymbol{e}_4\|_2^2 &= \partial_2 m_1 + \partial_1 m_2, \\
\lambda^{\mu} \sum_j \varepsilon f_j^{(1)} e_{5,j} / \|\boldsymbol{e}_5\|_2^2 &= \partial_3 m_2 + \partial_2 m_3, \\
\lambda^{\mu} \sum_j \varepsilon f_j^{(1)} e_{6,j} / \|\boldsymbol{e}_6\|_2^2 &= \partial_3 m_1 + \partial_1 m_3, \\
\lambda^{\mu} \sum_j \varepsilon f_j^{(1)} e_{7,j} / \|\boldsymbol{e}_7\|_2^2 &= \partial_1 m_1 - (\partial_2 m_2 + \partial_3 m_3)/2, \\
\lambda^{\mu} \sum_j \varepsilon f_j^{(1)} e_{8,j} / \|\boldsymbol{e}_8\|_2^2 &= (\partial_2 m_2 - \partial_3 m_3)/2.
\end{aligned}$$

Together with the incompressibility assumption $\partial_\alpha m_\alpha = 0$, this provides a uniquely solvable linear system of equations for the rate-of-strain tensor $\partial_\alpha m_\beta + \partial_\beta m_\alpha$, from which the shear rate

$$\dot{\gamma}(\boldsymbol{m}) = \sqrt{\frac{1}{2}(\partial_\beta m_\alpha + \partial_\alpha m_\beta)(\partial_\alpha m_\beta + \partial_\beta m_\alpha)}$$

can be directly calculated. In Eq. (3), F_α is constant and ρ is constant up to $\mathcal{O}\left(\varepsilon^2\right)$,[11,14] so

$$\dot{\gamma}(\boldsymbol{u}(t,\boldsymbol{x})) = \frac{\dot{\gamma}(\boldsymbol{m}(t,\boldsymbol{x}))}{\rho(t,\boldsymbol{x})} + \mathcal{O}\left(\varepsilon^2\right),$$

and Eq. (6) yields

$$\varepsilon f_j^{(1)} = f_j - f_j^{eq} + \mathcal{O}\left(\varepsilon^2\right).$$

As a consequence, the shear rate $\dot{\gamma}(\boldsymbol{u})$ can be determined directly from known quantities, without the need for numerical differentiation.

Once the shear rate is known at each lattice point, local viscosity can be determined via the Cross model (2) and inserted into Eq. (5). In this way, shear-thinning behaviour is modelled in the lattice Boltzmann simulations below.

5. NUMERICAL RESULTS

In the following, computational results obtained with the numerical method described in Section 4 will be presented. In particular, Section 5.1 contains results for a simple benchmark problem and demonstrates the difference in flow behaviour between shear-thinning fluids and Newtonian ones, while Section 5.2 deals with the simulation of a real liquid composite moulding.

5.1. Channel Flow

The aim of this Section is to demonstrate the qualitative difference in flow behaviour of shear-thinning fluids and fluids with constant viscosity. For this purpose, the flow of an artificial shear-thinning fluid with

$$\mu(\dot{\gamma}) = 0.0001 + \frac{0.01 - 0.0001}{1 + (80\dot{\gamma}(\boldsymbol{u}))^{1.3}}\ \text{Pa s} \tag{7}$$

is compared to an artificial Newtonian fluid with $\mu = 0.001$ Pa s. The benchmark considered here is flow through a 2D rectangular channel with solid boundaries at top and bottom and periodic boundaries at left and right. The distance between the plates is $32\,\mu$m. Initially, the fluid is at rest, and a constant force of $1000\,\text{N/m}^3$ pointing from left to right is

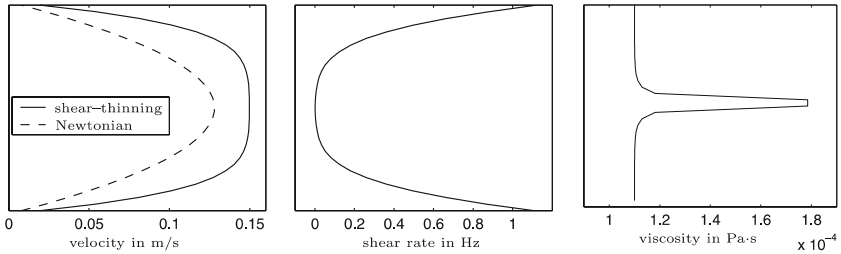

Fig. 2. Velocity profiles for shear-thinning and Newtonian flow (left) together with shear rate (middle) and viscosity (right) for shear-thinning flow in a 2D channel.

applied to induce the flow. Note that all those values are chosen exclusively for demonstrating shear-thinning effects and not to represent a realistic situation. Numerical simulation in a more realistic framework will be considered in Section 5.2.

Figure 2 shows the velocity profile of both fluids at stationary state together with shear rate and viscosity of the shear-thinning one at stationary state. While the Newtonian fluid exhibits the well-known parabolic velocity profile, the corresponding curve for shear-thinning flow is flattened around its maximum. Heuristically spoken, the reason why this happens is the following: The shear rate is equal to zero at the maximum of the velocity profile and is monotonously increasing towards the solid boundaries. Therefore, the viscosity has its maximum at the same position as the flow speed, i.e. in the centre of the channel, and is monotonously decreasing towards the solid boundaries. This behaviour of the viscosity allows the flow to speed up away from the centre of the channel.

The viscosity values applied here are chosen exclusively for the purpose of adequately exemplifying the qualitative difference of shear-thinning and Newtonian flow. Increasing or decreasing the viscosity of the Newtonian fluid would decrease respectively increase the maximum flow speed of the Newtonian fluid, while modifying (7) would change the quantitative behaviour of the shear-thinning flow.

5.2. Liquid Composite Moulding

In the present Section, some results from a joint project of Fraunhofer ITWM and Institut für Verbundwerkstoffe GmbH (IVW), Kaiserslautern, Germany, are presented.[19,20] The aim of this project is to model the injection of *in situ* polymerising polyamides into beds of carbon fibres, where *in situ polymerising* means the polyamides have already

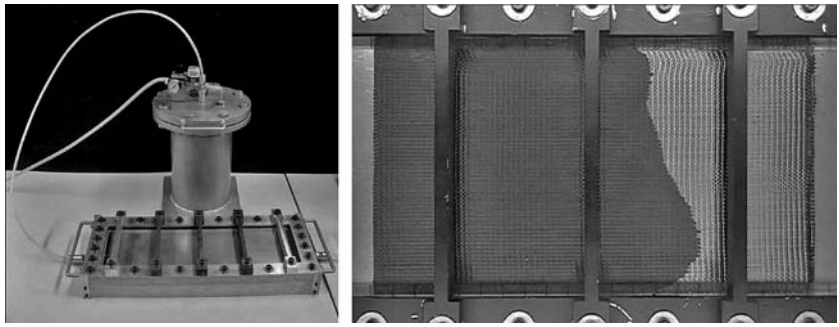

Fig. 3. The experimental apparatus used for the injection of polyamides in fibre beds. Left: the whole device consisting of the strictly fixed fibre bed, the liquid reservoir, and a system of flexible tubes. Right: top view of the partly saturated fibre bed, where the flow front is clearly visible. The pictures appear courtesy of IVW GmbH.

started to solidify when they are injected into the fibre bed. Injecting *in situ* polymerising polyamides into beds of carbon fibres is a typical way of producing reinforced plastic materials.

The simulations performed in this project are based on experiments done with the apparatus shown in Fig. 3. The flow in this experimental apparatus is driven by a pressure drop δp in x_3-direction and the simulations are performed for flow induced by a constant volume force. However, under the assumption that δp is constant over the length L of the flow system, pressure driven flow is equivalent to flow induced by the constant volume force $\mathbf{F} = (0, 0, \delta p/L)^T$.

In order to arrange a computer model of the flow channel, a solidified material sample produced in a laboratory experiment is cut along a line perpendicular to the flow direction, and highly resolved images of the cutting area are taken. Those images are then de-noised and extended to 3D space. The extended fibre bundles are considered to be rigid obstacles at fixed positions. Fig. 4 shows a grinding image of the fibre bed together with a virtual grinding image of the associated flow geometry. Note that single fibres are not resolved in the virtual flow geometry, only fibre bundles as a whole are taken into account. This is reasonable because the flow inside the fibre bundles is negligible compared to the flow between the fibre bundles.[16,19,20]

The fluid under investigation is the epoxy resin Ly 113/Hy 97, which is polymerising due to a chemical reaction. The shear-dependent viscosity of Ly 113/Hy 97 at different time intervals after the start of the chemical reaction is represented by the Cross models shown in Fig. 5, which are based on measurements performed at IVW.[19,20] In the following, the

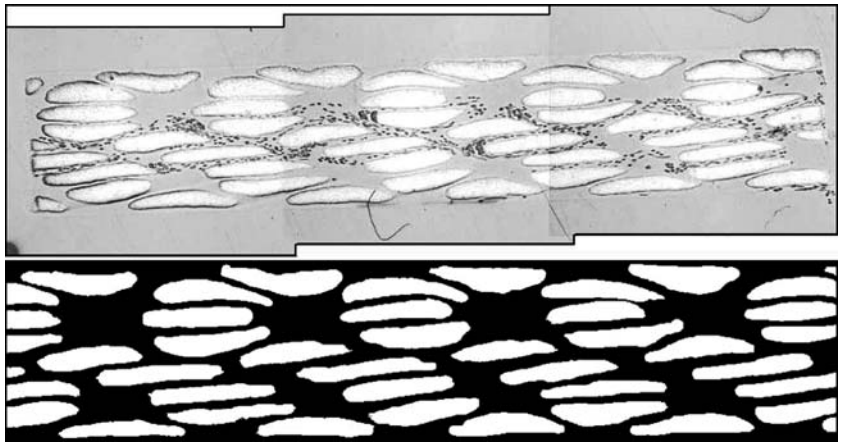

Fig. 4. Top: a grinding surface image of the fibre bed, where the bright spots mark the fibre bundles and the dark spots mark some air bubbles enclosed in the material probe (courtesy of IVW GmbH). Bottom: the associated digital model of the flow channel, where white marks the fibre bundles and black marks the flow channel. The lattice size is $1024 \times 224 \times 6$.

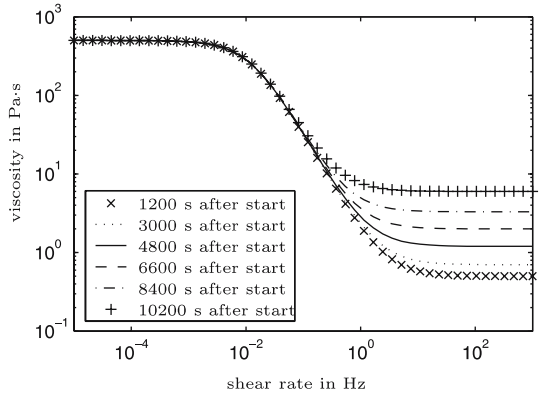

Fig. 5. Cross models for the viscosity function of Ly 113/Hy 97 at different time intervals after the start of the solidification. The functions are based on measurements performed at IVW.[19,20]

viscosity function measured 4800 s after the beginning of solidification, i.e.

$$\mu(\dot{\gamma}) = 1.2 + \frac{500 - 1.2}{1 + (80\dot{\gamma}(\boldsymbol{u}))^{1.3}} \text{ Pa s}$$

will be used to represent Ly 113/Hy 97. The chemical process of polymerisation is not considered here.

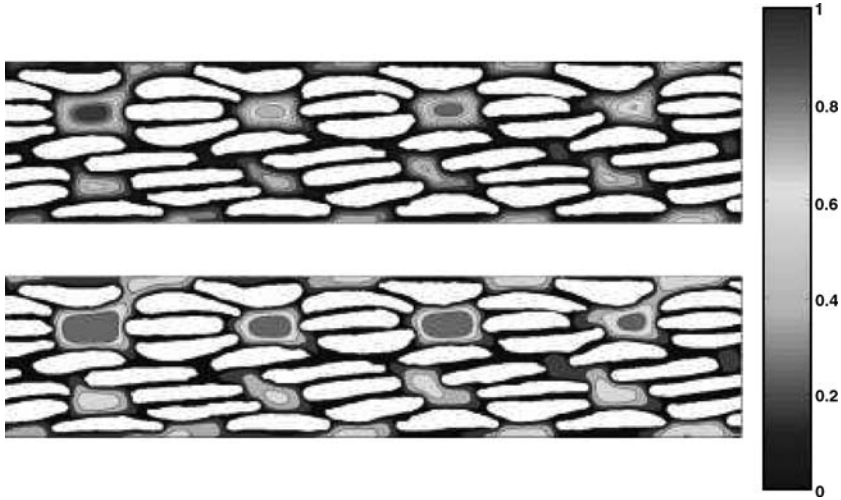

Fig. 6. Velocity field in the dimensionless unit $u/u_{\max}$ for a Newtonian fluid (top) and Ly 113/Hy 97 (bottom) in a bed of fibre bundles.

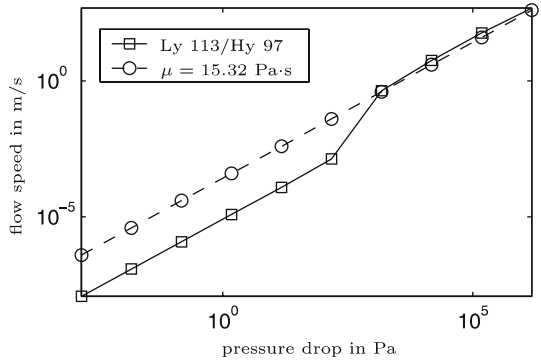

Fig. 7. Flow speed versus pressure drop for Ly 113/Hy 97 and a Newtonian fluid with $\mu = 15.32$ Pa s.

The behaviour of the epoxy resin will be compared to that of a Newtonian fluid with viscosity $\mu = 15.32$ Pa s. In analogy to Section 5.1, the Newtonian viscosity is chosen exclusively for the purpose of providing a useful comparison.

A qualitative comparison of flow fields for Ly 113/Hy 97 and the constant viscosity fluid is given in Fig. 6, and a corresponding quantitative plot of average flow speed versus pressure drop is given in Fig. 7. At low pressure drops, the viscosity of Ly 113/Hy 97 remains in the upper

Newtonian regime ($\mu = 500$ Pa s), thus inducing an average flow speed which is linearly increasing with pressure drop, in analogy to the flow speed of the Newtonian fluid. When the pressure drop is large enough, the shear-thinning effect eventually causes the average flow speed of the resin to increase until it reaches its lower Newtonian regime ($\mu = 1.2$ Pa s), where the average flow speed is higher than that of the Newtonian fluid. Note that the viscosity of the Newtonian fluid was chosen between the Newtonian limits of Ly 113/Hy 97 in order to effectively visualize the influence of shear-thinning behaviour on the speed–pressure diagram (Fig. 7).

6. CONCLUDING REMARKS

It was demonstrated how shear-thinning fluids can be easily modelled without necessity of numerical differentiation by following a lattice Boltzmann approach. The capability of this approach was underlined by numerical simulation of a simple benchmark problem and a real laboratory experiment. Computations for shear-thinning fluids are a field where lattice Boltzmann methods have clearly proven their practical usability for industrially relevant problems and their ability to compete with other numerical methods for simulating fluid flow.

The proposed mathematical model of shear-thinning fluids does not cover time-dependence of the viscosity function, so it is suitable only for rough qualitative simulation of *in situ* polymerising polyamides. Note, however, that local viscosity at each lattice point is directly computed in each time step from strictly local quantities, so time dependence of the Cross model can be introduced in a straightforward way. Furthermore, it would be worthwhile to replace the extended 2D geometries representing the fibre bundles used in liquid composite moulding by real 3D microstructures, but this task is left for future research.

ACKNOWLEDGMENTS

This work was supported by the Deutsche Forschungsgemeinschaft (German Research Foundation) in the project *Entwicklung einer Simulation für das Liquid Polymer Moulding, NE 269/13-1*. The author thanks Matthias Repsch and Ulrich Huber of the Institut für Verbundwerkstoffe for performing laboratory experiments and providing pictures of their experimental apparatus, his colleagues Stefan Rief and Konrad Steiner for their support and a lot of fruitful discussions, and the unknown referees for many helpful hints und suggestions.

REFERENCES

1. E. Aharonov and D. H. Rothman, Non-Newtonian flow (through porous media): A lattice Boltzmann method, *Geophys. Res. Lett.* **20**:679–682 (1993).
2. J. M. Buick and C. A. Greated, Gravity in a lattice Boltzmann model, *Phys. Rev. E* **61**:5307–5320 (2000).
3. M. M. Cross, Rheology of non-Newtonian fluids: A new flow equation for pseudo-plastic systems, *J. Colloid Sci.* **20**:417–437 (1965).
4. H. P. Darcy, *Les fontaines publiques de la ville de Dijon* (Dalmont, Paris, 1856).
5. U. Frisch, D. d'Humières, B. Hasslacher, P. Lallemand, Y. Pomeau, and J.-P. Rivet, Lattice gas hydrodynamics in two and three dimensions, *Complex Systems* **1**:649–707 (1987).
6. I. Ginzbourg and P. M. Adler, Boundary flow condition analysis for the three-dimensional lattice Boltzmann model, *J. Phys. II France* **4**:191–214 (1994).
7. I. Ginzburg and K. Steiner, A free-surface lattice Boltzmann method for modelling the filling of expanding cavities by Bingham fluids, *Phil. Trans. R. Soc. Lond. A* **360**:453–466 (2002).
8. I. Ginzburg and K. Steiner, Lattice Boltzmann model for free-surface flow and its application to filling process in casting, *J. Comput. Phys.* **185**:61–99 (2003).
9. L. Giraud, D. d'Humières, and P. Lallemand, A lattice Boltzmann model for visco-elasticity, *Int. J. Mod. Phys. C* **8**:805–815 (1997).
10. L. Giraud, D. d'Humières, and P. Lallemand, A lattice Boltzmann model for Jeffrey's visco-elastic fluid, *Europhys. Lett.* **42**:625–630 (1998).
11. X. He and L.-S. Luo, Lattice Boltzmann model for the incompressible Navier–Stokes equation, *J. Stat. Phys.* **88**:927–944 (1997).
12. D. d'Humières, Generalized lattice Boltzmann equations, in *Rarefied Gas Dynamics: Theory and Simulations* (Progress in Astronautics and Aeronautics **159** (1992), AIAA, Washington DC.), pp. 450–458.
13. D. d'Humières and P. Lallemand, Gaz sur réseau pour la représentation des ondes transverses, *C. R. Acad. Sci. Paris II* **317**:997–1001 (1993).
14. M. Junk, A finite difference interpretation of the lattice Boltzmann method, *Numer. Methods Partial Differ. Equations* **17**:383–402 (2001).
15. M. Junk and Z. Yang, Analysis of lattice Boltzmann boundary conditions, *PAMM* **3**:76–79 (2003), DOI 10.1002/pamm.200310320.
16. D. Kehrwald, Parallel lattice Boltzmann simulation of complex flows, in *Proceedings of the NAFEMS Seminar "Simulation of Complex Flows (CFD) – Applications and Trends"* (Niedernhausen bei Wiesbaden, Germany, 3–4 May 2004).
17. P. Lallemand, D. d'Humières, L.-S. Luo, and R. Rubinstein, Theory of the lattice Boltzmann equation: Three-dimensional model for linear visco-elastic fluids, *Phys. Rev. E* **67**:021203 (2003), DOI: 10.1103/PhysRevE.67.021023.
18. R. G. Owens and T. N. Phillips, *Computational Rheology* (Imperial College Press, London, 2002).
19. M. Repsch, U. Huber, M. Maier, S. Rief, D. Kehrwald, and K. Steiner, Process simulation of LPM (Liquid Polymer Moulding) in special consideration of fluid velocity and viscosity characteristics, accepted for publication in the Proceedings of FPCM-7 (Newark, DE, 7–9 July 2004).
20. M. Repsch, U. Huber, S. Rief, D. Kehrwald, and K. Steiner, New perceptions regarding the influence of RTM-process parameters on the microstructure of a non-crimp fibre fabric bed, submitted to *Composites Part A*.
21. D. H. Rothman and S. Zaleski, *Lattice-Gas Cellular Automata* (Cambridge University Press, Cambridge, 1997).

22. S. Succi, *The Lattice Boltzmann Equation for Fluid Dynamics and Beyond* (Clarendon Press, Oxford, 2001).
23. D. Wolf-Gladrow, *Lattice-Gas Cellular Automata and Lattice Boltzmann Models* (Springer, Berlin, 2000).
24. K. Yasuda, R. C. Armstrong, and R. E. Cohen, Shear flow properties of concentrated solutions of linear and star branched polysterones, *Rheol. Acta.* **20**:163–178 (1981).